J. Phys. B: At. Mol. Opt. Phys. **30** (1997) 1975–1988. Printed in the UK PII: S0953-4075(97)80398-7

Ab initio potential energy curves of Rydberg, valence and continuum states of NO

Ismanuel Rabadán and Jonathan Tennyson†

Department of Physics and Astronomy, University College London, Gower Street, London WC1E 6BT, UK

Received 19 December 1996

Abstract. Bound states and quasibound Rydberg states of NO are studied as a function of internuclear distances in the range 1.6–3.024 a_0. *R*-matrix calculations which include 12 configuration interaction target states in the close-coupling expansion are performed. Rydberg states of up to $n = 10$ are studied for the $^2\Sigma^+$, $^2\Pi$ and $^2\Delta$ symmetries of NO. Intruder states, of both valence and Rydberg character, are followed both above and below the ionization threshold. Where possible these states are classified as Rydberg states of an excited state of the ion. Away from avoided crossings, it is found that the quantum defects of the Rydberg series converging on the $X\,^1\Sigma^+$ state of NO^+ show little sensitivity to bondlength but show considerable dependence on the number of states included in the close-coupled expansion.

1. Introduction

Rydberg states in molecules are known to play a crucial role in the dissociative recombination (DR) process (Tennyson 1996a). In the case of NO, DR is relevant, for example, in the E and F region of the ionosphere, where NO^+ is one of the most abundant molecular ions (Wayne 1991) and the hot oxygen thus produced contributes to the maintenance of the night-time ionosphere (Shematovich and Bisikalo 1994). Furthermore, the bound Rydberg states of the NO molecule have attracted a good deal of attention for many years (Huber and Herzberg 1979) due, in part, to the simplicity of its structure. This simplicity is a consequence of the high first electronic excitation energy of NO^+ (6.5 eV, Albritton *et al* 1979), which means that the Rydberg series converging to the excited NO^+ states do not mix with the ground-state series, and the high ionization energy of NO (9.6 eV, Gilmore 1965), that facilitates the presence of low-*n* members of the Rydberg series.

Standard *ab initio* calculations of the potential energy curves of NO have been limited to the valence and low-lying Rydberg states (Vivie and Peyerimhoff 1988) due to the difficulty in describing the Rydberg electron, which requires very diffuse functions. On the other hand, *ab initio* scattering methods, such as the *R*-matrix method (Burke and Berrington 1993), are adept at describing a diffuse electron outside an ionic core but, traditionally, have lacked the high-level description of the core found in standard (bound) methods. This limitation has partially been removed with the development of new algorithms (Tennyson 1996b).

In a previous paper, henceforth known as I, Rabadán and Tennyson (1996) presented calculations of the bound and continuum states of the e^-–NO^+ system using the UK

† E-mail address: j.tennyson@ucl.ac.uk

0953-4075/97/081975+14$19.50

R-matrix package (Gillan *et al* 1995). Those calculations were performed at the NO equilibrium bondlength (2.175 a_0) and, in the best model, four configuration interaction (CI) target states were included in the close-coupling expansion.

In I, the bound states were parametrized using multichannel quantum defect theory (Seaton 1983, Moores and Saraph 1983). Quantum defects were obtained for $l \leqslant 5$, $m \leqslant 2$ and up to $n = 11$. The results were in reasonable quantitative agreement with experiment (Miescher and Huber 1976, Fredin *et al* 1987), although there was a systematic deviation of about 0.06 for all l waves. This deviation was ascribed to the effects of nuclear motion, which were omitted from the calculation, and/or insufficient correlation/polarization effects. In this work we address this issue by enlarging the close-coupling expansion to include up to 12 target states, improving the target representation and performing a series of fixed nuclei calculations in the internuclear distance range 1.6–3.024 a_0.

To extend the close-coupling expansion, we use the program SCATCI (Tennyson 1996b). This allows an increase in the complete active space (CAS) used in I. Furthermore, we also represent the target using natural orbitals instead of the SCF molecular orbitals of I. Both the CAS enlargement and the use of natural orbitals (NOs) improves the description of the target, especially the excited states. For the $N+1$ system, the best model we use has 12 CI target states, orthogonality relaxing configurations and correlation configurations.

Section 2 gives details of the theoretical treatment: description of the NO^+ target states, target plus electron description and how we get bound states and resonances. Section 3 presents results obtained at one geometry using different theoretical models, and at several geometries using a 12-state model. We conclude in section 4.

2. Calculation details

We use the molecular *R*-matrix method, details of which can be found in Huo and Gianturco (1995). The wavefunction in the inner region defined by a sphere of 15 a_0 centred on the centre of mass of the molecule is

$$\Psi_k = \mathcal{A} \sum_{i,j} a_{i,j,k} \Phi_i F_{i,j} + \sum_i b_{i,k} \chi_i \tag{1}$$

where $\mathcal{A}$ is the antisymmetrization operator, Φ_i are N-electron target wavefunctions, $F_{i,j}$ are continuum orbitals and χ_i are $N+1$-electron, two-centre, L^2 functions constructed from the target occupied and virtual molecular orbitals. In this work the target wavefunctions, Φ_i, are expressed as phase corrected (Tennyson 1997) CI expansions based on the use of CAS wavefunctions.

2.1. NO^+ target model

As in I, we start with a basis set of $(10\sigma, 6\pi, 1\delta, 1\phi)$ STOs (Billingsley 1975) centred on each nucleus. These orbitals are use to build a molecular basis of 16 orbitals, in which both the Φ_i and χ_i functions are expanded. As the molecular basis is smaller than the atomic basis, and we are restricted to the use of a single orbital set to expand all Φ_i target states, the energies of these states depend on the choice of the molecular orbitals. In the present work we employ NOs instead of the previous SCF ones.

To obtain the set of NOs, three SCF calculations were performed yielding a first molecular basis of $(20\sigma, 12\pi, 2\delta, 2\phi)$ SCF orbitals. From an SCF on $NO^+(X\,^1\Sigma^+)$ we select the first five σ orbitals, from an SCF on $NO^+(a\,^3\Sigma^+)$ the remaining σ orbitals and, finally, an SCF on $NO^+(A\,^1\Pi)$ produces the π, δ and ϕ orbitals. This SCF molecular basis

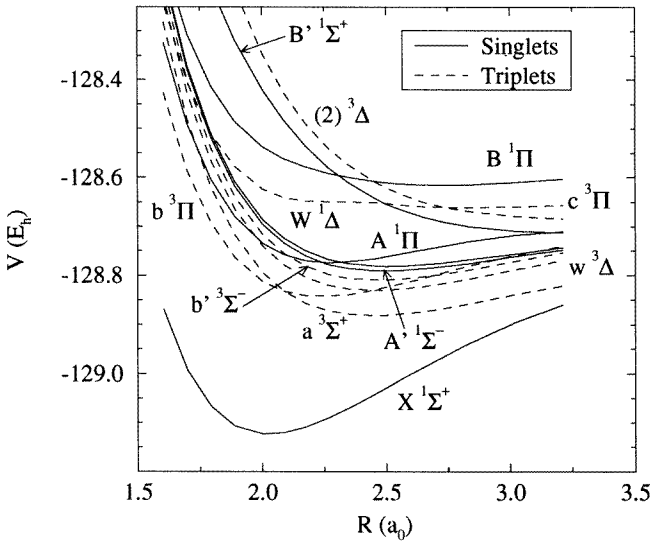

Figure 1. Calculated potential energy curves for the 12 lowest states of NO^+.

set is used in a CI calculation on $NO^+(X\,^1\Sigma^+)$ to get nine σ NOs and on $NO^+(A\,^1\Pi)$ to obtain five π, one δ and one ϕ NOs. In these CI calculations we used all configurations that arise moving 10 electrons in the CAS $(3\sigma, 4\sigma, 5\sigma, 6\sigma, 1\pi, 2\pi)$ and all single and double excitations from this CAS to the virtual space (7–20σ, 3–12π, 1–2δ, 1–2ϕ). The NOs calculations were performed using the ALCHEMY II programs (McLean *et al* 1991).

The largest target model in the present work contains 12 target states. The energy of these states as a function of the internuclear distance is shown in figure 1. Table 1 contains a comparison of the excitation energies at the equilibrium bondlength of NO (2.175 a_0) with calculations of I, Stratmann *et al* (1996), Partridge *et al* (1990) and experimental data of Albritton *et al* (1979). Present excitation energies are similar to the other calculations and within 5% of the experimental data.

2.2. NO system model

The continuum functions, $F_{i,j}$, that appear in equation (1) are partial wave expansions truncated to six waves and three symmetries ($m \leqslant 2$). Their radial part are the numerical solutions for an electron in an isotropic Coulomb potential, with an energy under 5 Ryd. With these conditions, we obtain 60 σ, 57 π and 54 δ functions, that were Schmidt orthogonalized to the set of NOs. Allowance is made for higher-energy solutions using a Buttle (1967) correction.

The L^2 functions (χ_i) used in the second sum in equation (1) were constructed similarly to the target wavefunctions (Φ_i): four electrons were frozen in the orbitals 1σ and 2σ giving a CAS of $(3\sigma, 4\sigma, 5\sigma, 6\sigma, 1\pi, 2\pi)$. The CAS was augmented by the 7–9σ, 3–5π, 1δ and 1ϕ virtual orbitals. All configurations arising from allocating: (i) 11 electrons in the CAS (orthogonality relaxing configurations) and (ii) 10 electrons in the CAS and one in the virtual space (correlation configurations) were included in the calculation.

In the outer region, defined by the sphere of 15 a_0, the scattered electron moves in the potential produced by the target charge, dipole and quadrupole moments. This potential included diagonal and off-diagonal terms between target states. The values of these

Table 1. Absolute energy (Hartree) of the ground state of NO^+ and vertical energy excitations (eV) for its first 11 excited states at $R = 2.175\ a_0$.

State	CSFs	This work	I[a]	Calculated[b]	Calculated[c]	Experimental[d]
$X\,^1\Sigma^+$	176	−129.1088	−129.0666			
$a\,^3\Sigma^+$	184	6.86	6.73	6.91	6.9	6.5
$b\,^3\Pi$	328	7.27	7.00	7.46	7.3	6.9
$w\,^3\Delta$	170	8.29	7.97	8.23	8.2	7.6
$b'\,^3\Sigma^-$	208	8.92		8.81	8.9	8.4
$A\,^1\Pi$	240	9.22		9.52	9.1	8.7
$A'\,^1\Sigma^-$	120	9.48		9.34	9.3	8.7
$W\,^1\Delta$	142	9.76		9.57	9.7	8.9
$c\,^3\Pi$	328	12.54		12.59	12.5	12.1
$B\,^1\Pi$	240	14.42		14.42	14.1	
$B'\,^1\Sigma^+$	176	15.62		15.36	14.7	13.4
$(2)\,^3\Delta$	170	16.87				

[a] Rabadán and Tennyson (1996).
[b] Stratmann *et al* (1996).
[c] Partridge *et al* (1990); values obtained by using the experimental ionization energy of 9.62 eV to fix the energy of the $NO^+(X\,^1\Sigma^+)$ state at this geometry.
[d] Albritton *et al* (1979).

multipoles for the ground state of NO^+ in the range 1.5–3.0 a_0 of internuclear distances are in good agreement with Fehér and Martin (1993) CASSCF calculations. In particular, at the NO^+ equilibrium geometry, our results for the dipole and quadrupole moments are 0.178 and 0.737 au respectively, to compare with interpolated Fehér and Martin's 0.15 and 0.74 au. Our dipole, none the less, does not decrease for bondlengths larger than 3 a_0 as does Fehér and Martin's, but remains almost constant up to 4 a_0 (the largest distance we have tried). This behaviour is probably a reflection of the quality of our target wavefunction at large bondlength and, therefore, we restrict the calculations in this work to distances up to 3 a_0.

2.3. Bound states

In the *R*-matrix method, bound states are expanded in terms of the inner region wavefunctions (1), which are used in the construction of the *R*-matrix. This matrix is propagated in the outer region (Morgan 1984) to 40 a_0, where the inner wavefunctions are matched with exponential decreasing functions obtained from a Gailitis expansion (Noble and Nesbet 1984).

The matching between inner and outer functions requires a scan in energies that is performed using the algorithm of Sarpal *et al* (1991) with the nonlinear grid in quantum defect of I. This grid takes advantage of the clustering of the Rydberg states around integer values of the effective quantum number due to the small quantum defect associated with higher partial waves. We had no problem locating all the bound states (up to six) associated with each n for each symmetry at most geometries.

As will be seen below, our calculations also revealed the presence of a number of intruder states perturbing the Rydberg series. These states are harder to find because their location is less predictable. The grid used proved flexible enough to locate many of these intruder states, particularly the important ones which lie in the low n region.

2.4. Resonances

The same information used to construct R-matrices for the bound states calculations can be employed to study continuum states of the system. In this case, the R-matrix was propagated in the outer region to 150 a_0, where the inner solutions are matched to a Gailitis expansion based on Coulomb functions (Noble and Nesbet 1984). The resonances detected were fitted to a Breit–Wigner profile using the program RESON (Tennyson and Noble 1984) to obtain their position (E_r) and width (Γ). In this work we concentrate on the lower-lying resonances. These resonances are important both for characterizing the intruder states in the bound Rydberg series and for dissociative recombination.

3. Results

3.1. Comparison between target models

In this work we introduce several improvements in the calculation compared with that employed in I. It is, therefore, worthwhile to examine the effect of these changes. This is done at the equilibrium distance of NO and for the total symmetry $^2\Pi$.

A convenient way to see these effects is by means of Edlén (1964) plots. For a particular Rydberg series, these plots compare quantum defect as a function of the energy ϵ, given as

$$\epsilon_{nl\lambda} = -\frac{1}{(n-\alpha_{nl\lambda})^2} \tag{2}$$

where n is the principal quantum number and $\alpha_{nl\lambda}$ is the quantum defect.

Figure 2(a) presents an Edlén plot for the pπ Rydberg series calculated with different models: (i) the four-state calculation of I that used SCF orbitals and the 'reduced' CAS $(4\sigma 5\sigma 6\sigma 1\pi 2\pi)^8$; (ii) the same model but using the NOs described in the previous section; (iii) a four-state model using the $(3\sigma 4\sigma 5\sigma 6\sigma 1\pi 2\pi)^{10}$ CAS and NOs; (iv) the same model incorporating eight additional target states (see table 1) to give a 12-state model; (v) the 12-state model with only the four states of the previous calculations included explicitly in the outer-region calculations. We note that model (v) is computationally significantly cheaper than model (iv). The first three models are magnified in the inset. The models are compared with the experimental results of Miescher and Huber (1976). Here, and elsewhere, experimental quantum defects refer to the lowest vibrational level of the Rydberg state concerned.

As in I, our quantum defects are systematically lower than the measured ones. It is seen that the main improvement, i.e. increase in quantum defect, comes from enlarging the close-coupling expansion. This improvement is retained when the eight higher target states are not included explicitly in the outer-region calculation. The change in quantum defects is small when NOs and/or the extended CAS (models in the inset) are used. These changes are more important for improving the representation of the excited target states (see table 1), which is crucial for obtaining intruder states in the correct position.

An important feature in figure 2(a) is a perturbation in the Rydberg series in the 12-state model. It will be shown below that this is caused by the presence of an intruder state in between the $n = 6$ and $n = 7$ states. The interaction between the intruder state and the Rydberg states stabilizes those states below the intruder, so increasing their quantum defect, and destabilizes those above, decreasing their quantum defect. The energy of the intruder state is strongly model dependent. In the four-state model, the intruder state appears above all Rydberg states calculated and its presence can be seen in the increase in quantum defect

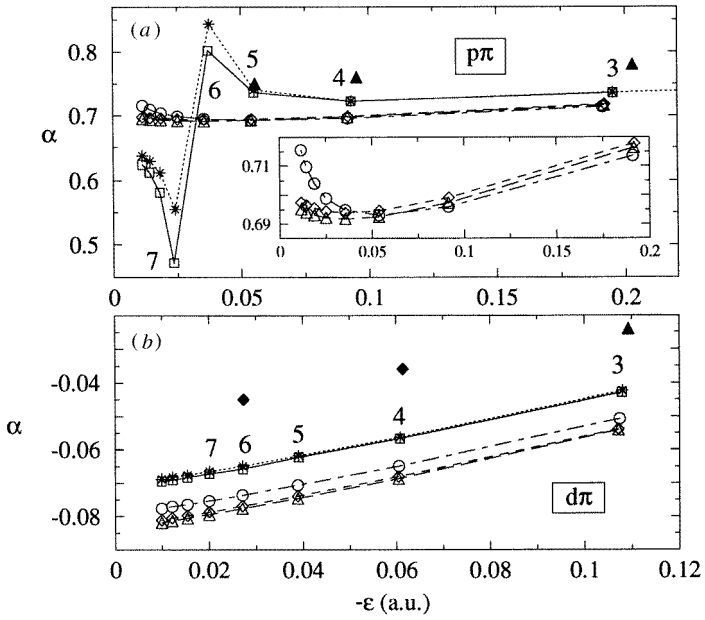

Figure 2. Edlén plot of the NO ($R = 2.175\ a_0$) Rydberg series of (a) pπ and (b) dπ symmetries for different models: ○, four-state model of I; △, four-state model with NOs and a 'reduced' CAS; ◇, four-state model; □, 12-state model; ∗, four-state model reduced from the 12-state model. Experiments: full triangle, Miescher and Huber (1976); full diamond, Fredin *et al* (1987). The numbers in the panels indicate the principal quantum number, n, of the states.

that these series show as $n \rightarrow 10$. This is the reason for the quadratic behaviour observed for this series in I.

The vertical ionization energies from the NO ground state (not included in figure 2(a)) and NO($C\,^2\Pi$) to $NO^+(X\,^1\Sigma^+)$, in the 12-state model, are 9.18 and 3.63 eV, and can be compared with experimental values 9.6 and 3.8 eV (Gilmore 1965). The NO ground state remains the least accurate state calculated due to its valence character; however, the corresponding figures in I were 8.71 and 3.56 eV, so the present calculation represents a significant improvement.

The other Rydberg series investigated show a more conventional behaviour, since they interact little with low intruder states (mainly of p character). As an example, we show the dπ series in figure 2(b). Here, it can again be seen that the biggest improvement is obtained by increasing the close-coupling expansion, and the results are not sensitive to including the eight higher states in the outer region calculation. The intruder state that produces the perturbation in series pπ seen in figure 2(a) shows no interaction with the series dπ.

Figure 3 contains Edlén plots for the series: sσ, pσ, dσ and dδ. Results with the 12-state model are compared with the four-state model in I and experimental data of Miescher and Huber (1976) and Fredin *et al* (1987). As in figures 2(a) and (b), the systematic difference between experimental and R-matrix results is reduced with the larger close-coupling. None the less, much of the difference still persists and, in the next subsection, we investigate the possible role of nuclear motion in the origin of this discrepancy.

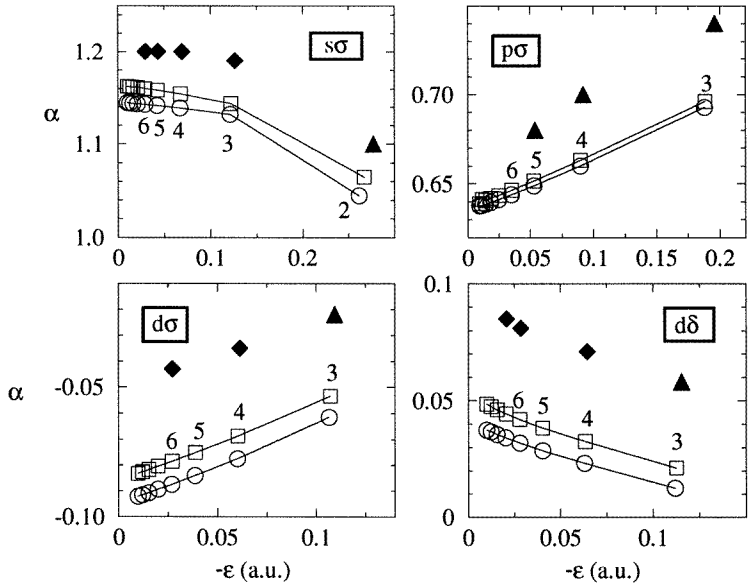

Figure 3. Edlén plot of the Rydberg series of the NO molecule at $R = 2.175\ a_0$. The series are indicated in each panel. R-matrix results: ○ , four-state model of I; □, 12-state model. Experiments: full triangle, Miescher and Huber (1976); full diamond, Fredin *et al* (1987). The numbers in the panels indicate the principal quantum number, n, of the states.

3.2. Geometry dependence

We have performed a series of fixed nuclei calculations (bondlengths $R = 1.606$, 1.701, 1.795, 1.890, 2.003, 2.089, 2.175, 2.268, 2.350, 2.457, 2.500, 2.560, 2.646, 2.736, 2.835 and 3.024 a_0) of the bound states of NO and lower resonances of e–NO^+ for total symmetries $^2\Sigma^+$, $^2\Pi$ and $^2\Delta$ using the 12-state model. These results are presented as potential energy curves, where the behaviour of the intruder states and their continuation into the continuum is clearly seen; plots of the effective quantum number v $(= n - \alpha_{nl\gamma})$ calculated from the NO^+ ground state as a function of R, which show the Rydberg structure and the interaction between Rydberg and intruder states; and the parameters of a linear fit to the Edlén plots for bondlengths between $R = 1.701$ and 2.457 a_0, that give information on the Rydberg behaviour of the series. The potential energy curve of the NO^+ ground state has been included in the figures displaying the potentials.

In a CI calculation, the states of the same symmetry do not cross. The avoided crossing produces a characteristic pattern that is more or less evident depending on the coupling between states and the coarseness of grid points calculated. Given that we use a fixed grid in internuclear distances for all calculations, we have diabatized the crossings between intruder and Rydberg states as well as those between resonances, when joining the energies at different geometries.

Figure 4 contains the potential energy curves of the states of symmetry $^2\Sigma^+$, three intruder states are identified and their continuation in the continuum spectrum as resonances can be clearly seen. In the discrete spectrum, some additional bound states have been obtained but not assigned to any series. The plot clearly shows a triple crossing between the two lower Rydberg states and the intruder state. We checked the valence origin of this intruder state by performing calculations for the geometries between $R = 2.457$ and

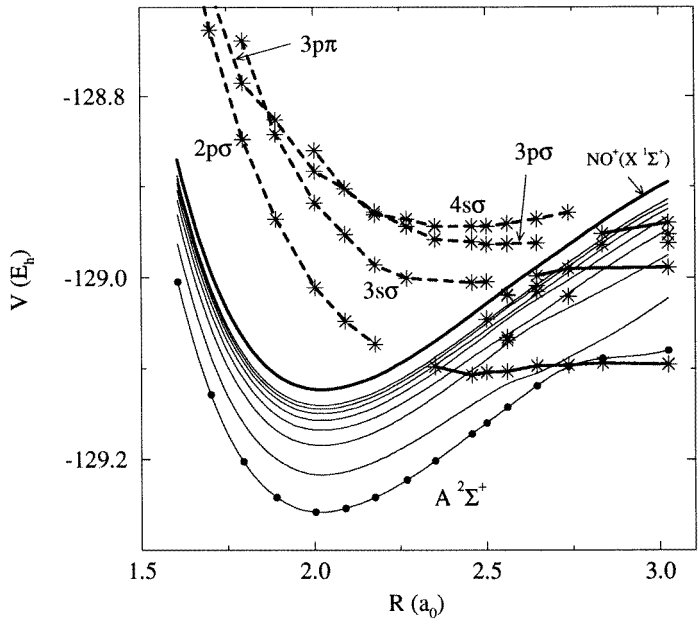

Figure 4. Potential energy curves of the $^2\Sigma^+$ states of NO. Full light curves: Rydberg states. The dots in the lowest state are the grid of geometries calculated. Only Rydberg states 3–6sσ and 3–6pσ are plotted. Stars mark the positions of the intruder states; full/broken curves join diabatically these states where bound/resonant.

3.024 a_0 that only included the NO^+ ground state in the close-coupling expansion. In that calculation, the lowest intruder state still appears, although it is 1.65 eV higher in energy.

The resonances are labelled in the figure according to their Rydberg series. Resonances with molecular character σ belong to the series converging to $NO^+(a\,^3\Sigma^+)$. The one labelled 3pπ belongs to the series converging to $NO^+(b\,^3\Pi)$ and only appears in this figure for internuclear distances smaller than 2.1 a_0. The quantum defects, α, obtained for these resonances are similar to those given in I at $R = 2.175\ a_0$. For the resonance 2pσ, $\alpha \simeq 0.5$ and its mean width, Γ, is 0.037 eV; the resonance 3sσ has $\alpha \simeq 1.0$ and $\Gamma \simeq 0.01$ eV; 3pσ has $\alpha \simeq 0.62$ and $\Gamma \simeq 0.01$ eV; finally, the resonance 4sσ has $\alpha \simeq 1.17$ and $\Gamma \simeq 0.002$ eV.

The 3sσ resonance is not detectable at $R = 2.350\ a_0$. To investigate the loss of this resonance, calculations that included only the $X\,^1\Sigma^+$ and $a\,^3\Sigma^+$ NO^+ states in the outer region were performed at geometries $R = 2.268$, 2.350 and 2.457 a_0. The resonance was found for all three geometries; at $R = 2.268$ and 2.457 a_0 it was very close in energy to the full calculation. Furthermore, in both calculations, the resonance undergoes a change in shape from a window at $R = 2.268\ a_0$ to a spike at $R = 2.457\ a_0$. This suggests that the loss of the resonance is not simply due to a change in the coupling between the discrete state and the continuum, but that coupling to higher electronic states is involved in the phenomenon.

The Rydberg structure of the $^2\Sigma^+$ series is displayed better in figure 5. Only Rydberg states with $l \leqslant 3$ are included in the plot because higher ones have very small quantum defects and do not show any visible features in this kind of graph. Intruder states have also been included. In this figure, the effect of the intruder states on the Rydberg series and the pattern of avoided crossing between Rydberg states are clear. These crossings are produced by the stabilization of the p wave; the crossings also mix the character of the

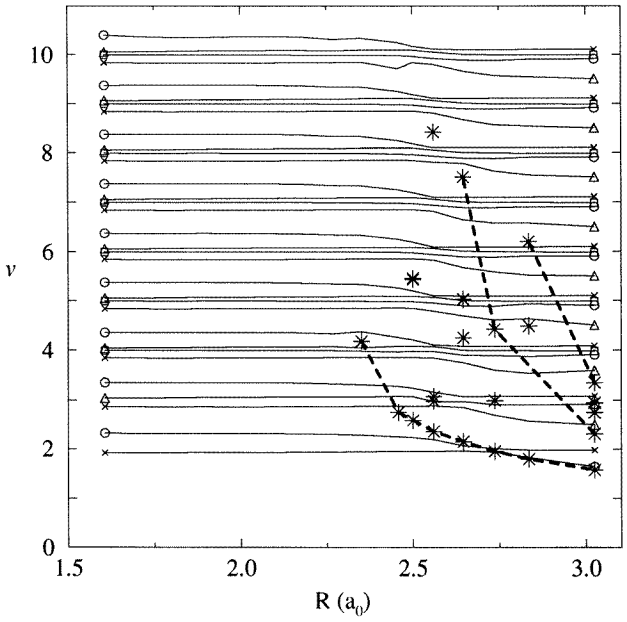

Figure 5. Effective quantum number, v (see text), of the NO($^2\Sigma^+$) bound states as a function of geometry. Included are the Rydberg states of $l \leqslant 3$. The l character of the states is indicated in the extremes. ×, s; ○ , p; △, d; □, f. Stars mark the position of the intruder states.

waves. The l character of the states is specified at the extremes of the curves and have been obtained by diagonalizing the matrix **S** at 0.3 eV above threshold (Seaton 1983, Tennyson 1988). An analysis of the figure shows that the presence of Rydberg states correlating with excited target states produce perturbations in the energy of the nearby Rydberg states. This interaction is, not surprisingly, larger when the states have the same l character.

The crossing between the lower two Rydberg states and the valence state in figures 4 and 5 has been analysed by Vivie and Peyerimhoff (1988). Even in their simplified model, their figure 2 demonstrates that this triple crossing is complicated. After exploring the variation with R of the NOs involved in these states, Vivie and Peyerimhoff (1988) conclude that the quasihomonuclear symmetry of the orbitals is lost as R increases. This facilitates the interaction between these Rydberg states, which is forbidden in homonuclear molecules.

Figure 5 shows a number of isolated intruder states. The effect of these states, as well as the intruder states for which we give curves, can be clearly seen on the Rydberg series. Of course the isolated intruder states should also lie on curves but these are difficult to construct with the limited bondlength-dependent information obtained here. A full study would require calculations at significantly more internuclear separations and was considered to be beyond the scope of this work.

Figure 6 gives the potential energy curves of the Rydberg, intruder and resonance states of total symmetry $^2\Pi$. The lower two intruder states also appear in a one-state calculation, but displaced towards higher energies 2.2 and 1.4 eV respectively. These displacements are large compared to the 0.02 eV of increase in the lower Rydberg states.

The lowest three intruder states, and their continuation as resonances, do not track any of the excited ionic-state curves, thus no labels have been assigned to them. This indicates that these states have a high 'valence' character. The resonance labelled 3sσ is

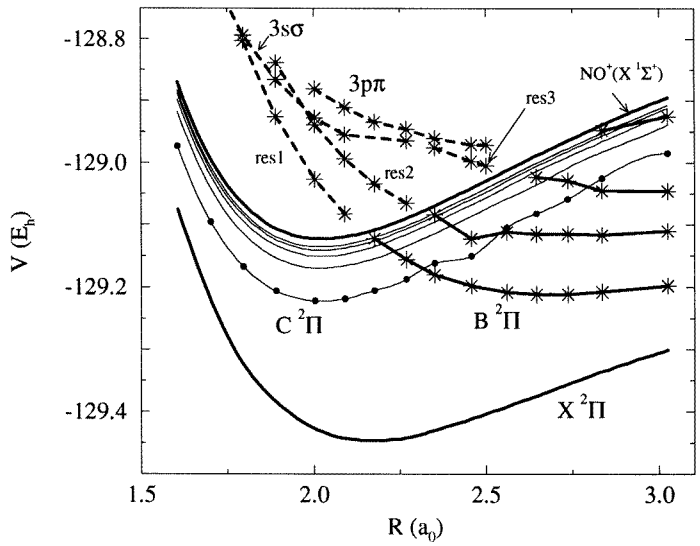

Figure 6. Potential energy curves of the $^2\Pi$ states of NO. Full light curves: Rydberg states. The dots in the C $^2\Pi$ state are the grid of geometries calculated. Only Rydberg states 3–7pπ are plotted. Stars mark the position of the intruder states; heavy full/broken curves join diabatically these states where bound/resonant.

from the series converging to $NO^+(b\,^3\Pi)$; its quantum defect is $\simeq 1.0$ and its width is about 0.06 eV. The 3pπ resonance is from the series converging to $NO^+(a\,^3\Sigma^+)$ and has $\alpha \simeq 0.6$ and $\Gamma \simeq 0.02$ eV. The three lowest intruder states have widths above threshold, from the lowest upwards, of about 0.07, 0.008 and 0.16 eV.

The coupling between the intruder states and the lowest Rydberg state, NO(C $^2\Pi$), appears strong and large interactions occur in the crossings.

Figure 7 gives the Rydberg states of symmetry $^2\Pi$ and their interactions with the valence states discussed above. Again, only Rydberg states with $l \leqslant 3$ are plotted. The three lowest intruder states produce mainly p-wave perturbations. The lowest (only) intruder state at $R = 2.175\ a_0$ appears at $v = 5.9$; it is the one that produce the perturbation in the p series seen in figure 2(*a*). Similar effects can be found at other geometries where intruder states appear. Indeed, this perturbation in the Edlén plots of a Rydberg series can be used to check that no intruder state has been missed in the energy span of the Rydberg series. This appears to be the case in the $^2\Pi$ symmetry where we appear to have isolated all the curves of the significant intruder states.

Figure 8 gives the potential curves of the Rydberg states and resonances of symmetry $^2\Delta$. Only one intruder state is found with this symmetry. It can be assigned to the first state of the Rydberg series sσ converging to $NO^+(w\,^3\Delta)$, with a quantum defect of about 0.68 and, above threshold, a width of 0.07 eV.

Unlike the lower symmetries, we do not give a figure of effective quantum number as a function of geometry for the $^2\Delta$ symmetry. The quantum defects of all Rydberg states are small, there are no s and p waves in this symmetry, and show little dependence on R. Furthermore, they do not show any perturbations visible on the scale of the plot.

More detailed information on the quantum defects of the Rydberg series, including the high-l waves, is presented in figure 9. This displays the parameters used to fit the

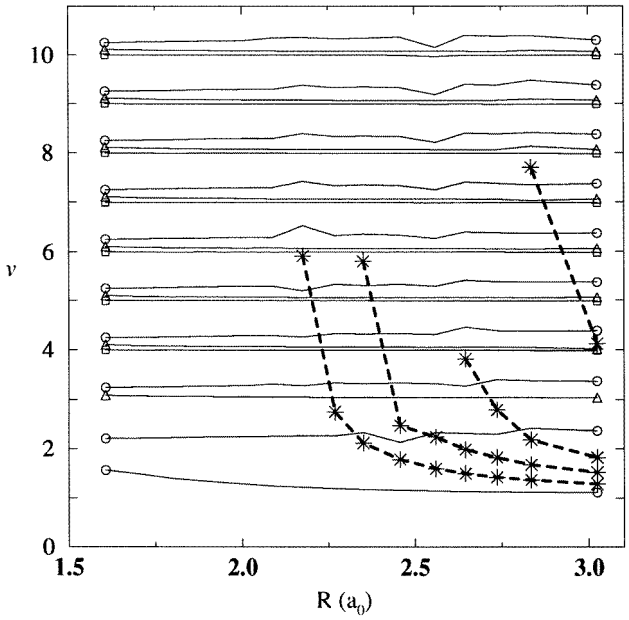

Figure 7. Effective quantum number, v (see text), of the NO($^2\Pi$) bound states as a function of geometry. Symbols are the same as figure 5.

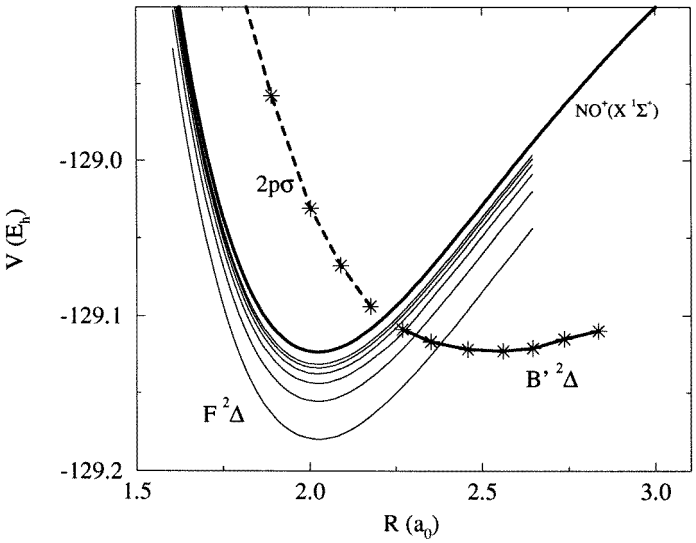

Figure 8. Energy diagram of the $^2\Delta$ states of NO. Full light curves: Rydberg states. Only Rydberg states 3–8dδ are plotted. Stars mark the position of the intruder state; heavy full/broken curves join diabatically this state where bound/resonant.

linear equation

$$\alpha = -a\epsilon + b \tag{3}$$

to the Edlén plots of the Rydberg series s–h for geometries between $R = 1.701$ and 2.457 a_0.

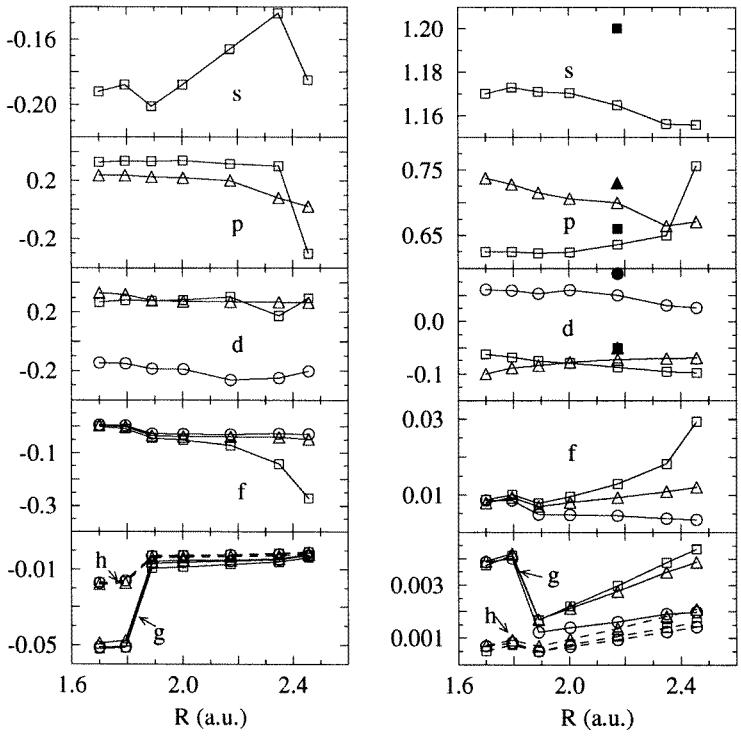

Figure 9. Edlén parameters $a(R)$ (left column) and $b(R)$ (right column) obtained from linear fits to equation (3). The l-character of the Rydberg series is indicated in the panels. □, Rydberg series of symmetry $^2\Sigma^+$; △, $^2\Pi$; ○ , $^2\Delta$. Full symbols are estimates from the experimental results shown in figures 2 and 3.

At $R = 2.175\ a_0$, estimates of b from the experimental data shown in figures 2 and 3 are included as full symbols. For larger values of R, the presence of intruder states produces perturbations in the Rydberg series (especially of the $^2\Sigma^+$ symmetry) and fitting to (3) is unphysical.

The actual quantum defects, as a function of n, are obtained from equations (2) and (3), at first order, as

$$\alpha_n = \frac{na + n^3 b}{n^3 - 2a}. \tag{4}$$

Figure 9 shows that the quantum defects become symmetry independent as l increases, especially at short bondlengths. Geometry dependence in the s wave is smaller than in the p wave (note the different scales). The largest changes, both in a and b, appear at $R = 2.457\ a_0$ in the p wave for the $^2\Sigma^+$ symmetry. This corresponds to the stabilization seen in figure 5 for this wave. The decrease in b as R increases for the p wave and $^2\Pi$ symmetry reflects the destabilization of the p wave in figure 7. We note a jump in the g wave and, to a lesser extent, the f and h waves between $R = 1.795$ and $1.890\ a_0$. This coincides with the quadrupole moment of $NO^+(X\,^1\Sigma^+)$ going through zero between these two geometries.

In figures 5, 7 and especially 9, it can be seen that our quantum defects are lower than the experimental ones, at least for geometries in the vicinity of the NO and NO^+ equilibrium. Furthermore, the quantum defects do not change with R in a way that would

suggest that the inclusion of nuclear motion in our calculation would significantly reduce the difference found between experimental and the theoretical quantum defects presented here and in I.

4. Conclusion

Using the *R*-matrix method, *ab initio* adiabatic curves for the NO Rydberg states of symmetries $^2\Sigma^+$, $^2\Pi$ and $^2\Delta$ have been calculated for a range of geometries extending well outside the NO and NO^+ equilibrium separations. Other bound states have been found and followed into the continuum spectrum as resonances. Some of these intruder states are clearly Rydberg states of an excited ionic state. In that case, the Rydberg character has been specified and a mean quantum defect given. For all resonances, the mean width has also been given. Tabulations of our data as a function of geometry are available from the authors†.

A comparison of models differing in the target representation and close-coupling expansion employed has been made. The calculated quantum defects proved sensitive to enlarging the close-coupling expansion. Conversely, the representation of individual target states proved more important for absolute energies, representing excited target states and, hence, for correctly positioning the crossings between the Rydberg series of the NO^+ ground estate and excited states. The large close-coupling was also important for the description of intruder states of valence character, which are to be important in dissociative recombination processes. For this mechanism, valuable information can be obtained from the valence–Rydberg interactions shown.

In I, we raised the possibility that the systematic differences between our calculated and the observed quantum defects might be due to our neglect of nuclear motion. This work shows that, away from avoided crossings, the quantum defects are hardly sensitive to the geometry. What is required is a better treatment of the polarization interactions via the close-coupling expansion and/or the CI expansion. In particular, one could include single and double excitations from the CAS (or a reduced version of it) to the virtual space. This possibility has been explored for Rydberg states of CO (Tennyson 1996c) with encouraging results.

Acknowledgments

We thank Lesley Morgan for many helpful discussions. This work was supported by the UK Engineering and Physical Sciences Research Council under grants GR/K47702 and GR/K89214.

References

Albritton D L, Schmeltekopf A L and Zare R N 1979 *J. Chem. Phys.* **71** 3271
Billingsley F P II 1975 *J. Chem. Phys.* **3** 864
Burke P G and Berrington K A (ed) 1993 *Atomic and Molecular Processes: An R-matrix Approach* (Bristol: IOP)
Buttle P J A 1967 *Phys. Rev.* **160** 719
Edlén B 1964 *Handbuch der Physik* vol 27 (Berlin: Springer)
Fehér M and Martin P A 1993 *Chem. Phys. Lett.* **215** 565
Fredin S, Gauyacq D, Horani M, Jungen C, Lefevre G and Masnou-Seeuws F 1987 *Mol. Phys.* **60** 825

† By anonymous ftp to jonny.phys.ucl.ac.uk from directory pub/astrodata/NO+, or via our www pages on http://jonny.phys.ucl.ac.uk/home.html

Gillan C J, Tennyson J and Burke P G 1995 *Computational Methods for Electron–Molecule Collisions* ed W M Huo and F A Gianturco (New York: Plenum)
Gilmore F R 1965 *J. Quant. Spectrosc. Radiat. Transfer* **5** 369
Huber K P and Herzberg G 1979 *Molecular Spectra and Molecular Structure. Vol 4. Constants of Diatomic Molecules* (New York: Van Nostrand)
Huo W M and Gianturco F A (ed) 1995 *Computational Methods for Electron–Molecule Collisions* (New York: Plenum)
McLean A D, Yoshimine M, Lengsfield B H, Bagus P S and Liu B 1991 *MOTECC: Modern Techniques in Computational Chemistry* ed E Clementi (Kingston, NY: IBM) ch 6
Miescher E and Huber K P 1976 *International Review of Science (Physical Chemistry Series Two)* vol 3 (London: Butterworth)
Moores D L and Saraph H E 1983 *Atoms in Astrophysics* (New York: Plenum)
Morgan L A 1984 *Comput. Phys. Commun.* **31** 419
Noble C J and Nesbet R K 1984 *Comput. Phys. Commun.* **33** 399
Partridge H, Langhoff S R and Bauschlicher C W Jr 1990 *J. Chem. Phys.* **93** 7179
Rabadán I and Tennyson J 1996 *J. Phys. B: At. Mol. Opt. Phys.* **29** 3747
Sarpal B K, Branchett S E, Tennyson J and Morgan L A 1991 *J. Phys. B: At. Mol. Opt. Phys.* **24** 3685
Seaton M J 1983 *Rep. Prog. Phys.* **46** 167
Shematovich V I and Bisikalo D V 1994 *J. Geophys. Res.* **29** 23 217
Stratmann R E, Zurales R W and Lucchese R R 1996 *J. Chem. Phys.* **104** 8989
Tennyson J 1988 *J. Phys. B: At. Mol. Opt. Phys.* **21** 805
——1996a *Comment. At. Mol. Phys.* **32** 209
——1996b *J. Phys. B: At. Mol. Opt. Phys.* **29** 1817
——1996c *J. Phys. B: At. Mol. Opt. Phys.* **29** 6185
——1997 *Comput. Phys. Commun.* in press
Tennyson J and Noble C J 1984 *Comput. Phys. Commun.* **33** 421
Vivie R and Peyerimhoff S D 1988 *J. Chem. Phys.* **89** 3028
Wayne R P 1991 *Chemistry of Atmospheres* 2nd edn (Oxford: Clarendon)